MOEM

Modern Electronic Materials 2019; 5(4): 151–157
DOI 10.3897/j.moem.5.4.52810

Research Article

Evaluation of crystallographic ordering degree of magnetically active ions in $Sr_2FeMoO_{6-\delta}$ by means of the (101) X-ray peak intensity

Evgenij Artsiukh[1], Gunnar Suchaneck[2]

1 SSPA «Scientific-Practical Materials Research Centre of NAS of Belarus», 19 P. Brovki Str., Minsk 220072, Belarus

2 TU Dresden, Solid State Electronics Laboratory, Dresden 01062, Germany

Corresponding author: Evgenij Artsiukh (sirfranzferdinand@yandex.ru)

Received 30 September 2019 ♦ **Accepted** 3 December 2019 ♦ **Published** 31 December 2019

Citation: Artsiukh E, Suchaneck G (2019) Evaluation of crystallographic ordering degree of magnetically active ions in $Sr_2FeMoO_{6-\delta}$ by means of the (101) X-ray peak intensity. Modern Electronic Materials 5(4): 151–157. https://doi.org/10.3897/j.moem.5.4.52810

Abstract

Strontium ferromolybdate double perovskite is a promising candidate for room-temperature spintronic applications. Nevertheless, SFMO has not yet found wide application in spintronics. This is attributed to the low reproducibility of its magnetic properties which partially originates from their strong dependence on the ordering degree of Fe and Mo ions in the B' and B'' sublattices of double perovskite $A_2B'B''O_6$.

In this work, we have considered an express method of determining the degree of disorder in strontium ferromolybdate. The sublattice occupation with Fe and Mo ions has been estimated for stoichiometric and nonstoichiometric $Sr_2FeMoO_{6-\delta}$ with a 5% Fe and Mo excess, respectively. We have calculated the intensity ratio between the superstructure (101) XRD peak and the most intense (112 + 200) peak. The calculated curves have been fitted to an analytical expression of a similar case known from literature. The calculation results obtained using the proposed method are within a ± 25 % agreement with Rietveld analysis of experimental data. Thus, this method can be used as an alternative to Rietveld analysis if the exposure time during X-ray diffraction experiment was insufficient. We have discussed the dependence of the $I(101)/I(112 + 200)$ peak intensity ratio on various factors including instrumental broadening of diffraction peaks, peak twinning due to grain size reduction, thin film lattice parameter variation due to substrate lattice mismatch and lattice parameter variation due to oxygen vacancies.

The relevance of the method is the evaluation of the degree of superstructure ordering in $Sr_2FeMoO_{6-\delta}$ without large time consumption for X-ray diffraction pattern recording and Rietveld data processing which may be essential when dealing with large amounts of experimental data.

Keywords

strontium ferromolybdate, atomic ordering degree, X-ray structural analysis

1. Introduction

Strontium ferromolybdate ($Sr_2FeMoO_{6-\delta}$, **SFMO**) double perovskite is a promising candidate for room-temperature spintronic applications since it possesses a half-metallic character with theoretically 100% spin polarization [1] and a high Curie temperature of about 415 K enabling its application at room temperature (ferrimagnets should

be operated in their ordered magnetic state below the Curie point). Additionally, SFMO exhibits a sufficient low-field magnetoresistance **(LFMR)** [2]. The LFMR is almost absent in single crystals [3] and reaches 6.5% in highly-ordered ceramics at room temperature when applying a magnetic flux density of 0.3 T [4]. Nevertheless, SFMO has not yet found wide application in spintronics. This is attributed to the low reproducibility of its magnetic properties which partially originates from their strong dependence on the ordering degree of Fe and Mo ions in the B' and B'' sublattices of double perovskite $A_2B'B''O_6$ [5].

SFMO possesses a tetragonal structure with the $I4/m$ space symmetry group. However, some authors favor a space group $I4/mmm$ with a lowered symmetry [6–9]. The perfect Sr_2FeMoO_6 lattice structure can be considered as a modified perovskite structure in which corner connected FeO_6 and MoO_6 octahedra with cubic or tetragonal symmetry alternate along the three cubic axes. Cations A are in the cubic octahedral voids formed by the FeO_6 and MoO_6 octahedra (Fig. 1). The ordering degree S of stoichiometric SFMO is determined by the fraction of ions in the "wrong" sublattice, i.e., the so-called antisite disorder [10]

$$S = 1 - 2\mathrm{ASD}. \tag{1}$$

Antisite disorder **(ASD)** takes place if a Fe ion from the Fe sublattice occupies a Mo ion site in the Mo sublattice (Fe_{Mo}) and vice versa (Mo_{Fe}). Thus, ASD is distinguished by the formation of Fe_{Mo} and Mo_{Fe} defect pairs. The ASD value may vary from 0 (complete order) to 0.5 (random distribution of Fe and Mo ions in the sublattices). Additionally, single antisite defects may occur if, e.g., excess Fe ions occupy sites in the Mo sublattice to form Fe_{Mo} [11].

In the perfect SFMO lattice, the (101) crystallographic planes are the ones of either Fe or Mo. Correspondingly, a (101) superstructure peak appears in the X-ray diffraction pattern. The intensity of the (101) superstructure peak decreases with the development of ASD. It disappears completely in disordered structures where Fe and Mo ions are distributed randomly between the sublattices. Another superstructure reflection is the (103) peak. However, its intensity is far lower than that of the (101) peak even in a completely ordered material [12].

On the other hand, the SFMO lattice contains planes whose diffraction peak intensities do not depend on the degree of cation ordering in the B-site sublattices. Therefore, they can be used for comparison with the (101) superstructure peak intensity in order to determine the degree of antisite disorder. In literature, the double (112) + (200) peak [6] or the (404) peak [14] are used for such calibration. The (112) diffraction peak is the most intense one in SFMO and hence its intensity can be determined with the least errors. On the other hand, it partially overlaps with the (200) peak. This should be taken into account in the analysis.

For the first time, the $I(101)/[I(112) + I(200)]$ X-ray peak intensity ratio was used for ASD evaluation in the Fe and Mo sublattices in [6]. Later, this ratio was considered in [7, 15]. Thereby, it was assumed that the $I(101)/[I(112) + I(200)]$ peak intensity ratio decreases linearly with increasing disorder [7]. Afterwards, the $I(101)/[I(112) + I(200)]$ peak intensity ratio was widely used as a measure of disorder in SFMO ceramic specimens [17–20].

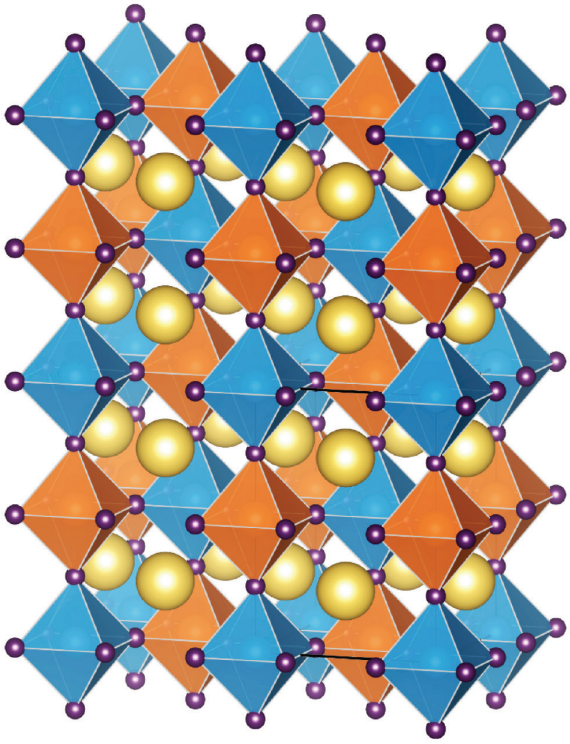

Figure 1. Perfect SFMO crystal lattice (Sr ions are marked in yellow, Fe ions in blue, Mo ions in orange and O ions in purple). The image was obtained by means of VESTA software [13].

Antisite disorder was evaluated also by 2D mapping of reciprocal space for the (101) and (404) peaks [14]. The $I(101)/I(404)$ peak integral intensity ratio was taken as a measure of disorder in the sublattices using the following expression:

$$\mathrm{ASD} = b - \sqrt{\frac{I(101)}{aI(404)}}, \tag{2}$$

where $a = 0.5583 \pm 0.0005$ and $b = 0.5225 \pm 0.0002$ are constants obtained by X-ray pattern simulation [14].

In our case of the $I(101)/[I(112) + I(200)]$ peak intensity ratio, there is no theoretical formula which could be used for evaluating disorder degree avoiding preliminary X-ray pattern treatment by means of the Rietveld method. This gap is closed in this work.

2. Theory

In the following, we consider the intensity I of a X-ray reflection estimated as the height of the corresponding peak since this parameter can be reliably measured even if the X-ray exposure time is short. For example, the exposure

Table 1. Ion positions in the SFMO lattice [8].

Ion	Position		
	X	*Y*	*Z*
Sr	0.5	0	0.5
Fe_{Fe}	0	0	0
Fe_{Mo}	0	0	0
Mo_{Mo}	0	0	0
Mo_{Fe}	0	0	0
O1	0	0	0.5
O2	0.25	0.5	0

Notations: Fe_{Fe} and Fe_{Mo} are the Fe ion positions in the Fe and Mo sublattices, and Mo_{Mo} and Mo_{Fe} the molybdenum ion positions in the Mo and Fe sublattices, respectively.

time required for a reliable full-profile analysis of X-ray diffraction patterns is one order of magnitude larger than that required for phase analysis [21]. This makes Rietveld analysis of X-ray pattern quite time-consuming.

The calculations were carried out using the VESTA [13] and RIETAN-FP·VENUS Package [22] software. The initial data for SFMO X-ray diffraction pattern simulation (Table 1) were taken from an earlier work [8]. A SFMO cell with *I*4/*m* space group was considered as the main structure. The assumed lattice parameters were a = 0.557 nm and c = 0.790 nm. The radiation was CuK_α (wavelength 0.154059 nm).

The main point defects in SFMO synthesized under oxygen deficiency are Sr vacancies and antisite defects [23]. Therefore, for simplicity, we will consider in the following Fe and Mo sublattices completely occupied by Fe or Mo ions.

The ordering degree in stoichiometric SFMO is given by

$$S = Fe_{Fe} - Fe_{Mo} = Mo_{Mo} - Mo_{Fe}. \quad (3)$$

In this case, the degree of sublattice occupation with Fe and Mo cations is determined by the following formulae:

$$Fe_{Fe} = 1 - \left(\frac{100 - ASD}{100\%}\right); Fe_{Mo} = 1 - Fe_{Fe} \quad (4)$$

$$Mo_{Mo} = 1 - \left(\frac{100 - ASD}{100\%}\right); Mo_{Fe} = 1 - Mo_{Mo} \quad (5)$$

In nonstoichiometric $Sr_2Fe_{1-x}Mo_{1+x}O_{6-\delta}$, the degrees of sublattice occupation with Fe and Mo cations are determined as follows [24]

$$Fe_{Fe} = (1-x)\left(\frac{100 - ASD}{100\%}\right); Fe_{Mo} = (1-x) - Fe_{Fe} \quad (6)$$

$$Mo_{Mo} = x + (1-x)\left(\frac{100 - ASD}{100\%}\right); Mo_{Fe} = 1 + x - Mo_{Mo} \quad (7)$$

and correspondingly in $Sr_2Fe_{1+x}Mo_{1-x}O_{6-\delta}$:

$$Fe_{Fe} = x + (1-x)\left(\frac{100 - ASD}{100\%}\right); Fe_{Mo} = 1 + x - Fe_{Fe} \quad (8)$$

$$Mo_{Mo} = (1-x)\left(\frac{100 - ASD}{100\%}\right); Mo_{Fe} = (1-x) - Mo_{Mo} \quad (9)$$

In order to determine ASD as a function of the $I(101)/[I(112) + I(200)]$ peak intensity ratio, we have used the sublattice occupation data compiled in Tables 2–4.

3. Results and discussion

The comparison of the calculated ASD as a function of the $I(101)/[I(112) + I(200)]$ peak intensity ratio with experimental data is shown in Fig. 2. Along with data for high-temperature sintered ceramics, i.e., coarse-grained ones [6, 16, 18], sparse data [9, 25–32] were also taken into account.

For the simulated SFMO crystal with the described above parameters (*I*4/*m*, a = 0.557 nm and c = 0.790 nm), the (101) peak for CuK_α radiation is located at 19.484°, the (112) peak at 32.066° and the (200) peak is shifted to a higher angle beyond the (112) peak by 0.047°. Accounting only the (112) peak, overestimates the ASD in comparison with the literature data. With regard to the very small difference in the (112) and (200) peak positions, the sum of the (112) + (200) peak intensities may be considered as 149.8% of the (112) peak intensity.

The total peak intensity depends on a number of factors:

- instrumental broadening of diffraction peaks;
- peak broadening due to grain size reduction;
- thin film lattice parameter variation due to substrate lattice mismatch;
- lattice parameter variation due to oxygen vacancies etc.

We will now consider these factors more in detail.

Instrumental broadening of diffraction peaks can be evaluated experimentally using the NIST-Si-standard 640d [33]. For example, for a Bruker D8 Discover X-ray spectrometer in Bragg–Brentano setup, the instrumental broadening of diffraction peaks at low diffraction angles is approx. 0.17°. Consequently, the total intensity of the (112) + (200) peaks increases to 146.5% of the (112) peak intensity. The peak broadening due to grain size reduction

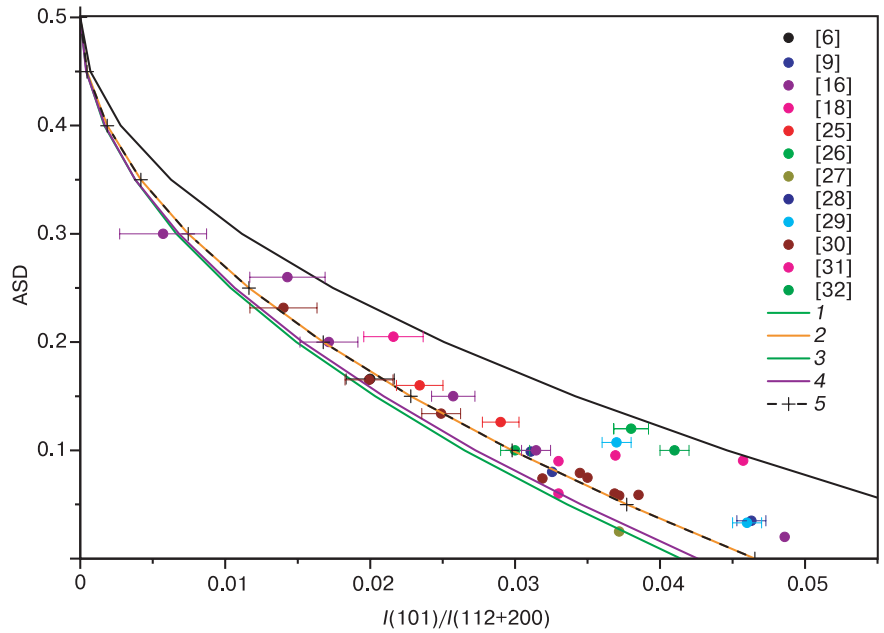

Figure 2. Comparison of the ASD (*1*–*5*) calculated as a function of (101) peak intensity ratio with literature data of Rietveld analysis of X-ray diffraction patterns [6], [9], [16], [18], [25–32]: (*1*) calculation excluding the (200) peak, (*2*) calculation for the sum of (112) and (200) peak intensities, (*3*) calculation for the sum of (112) and (200) peak intensities for $Sr_2Fe_{0.95}Mo_{1.05}O_{6-\delta}$ (*4*) calculation for the sum of (112) and (200) peak intensities for $Sr_2Fe_{1.05}Mo_{0.95}O_{6-\delta}$ and (*5*) calculation using Eq. (11).

Table 2. Ion occupation in the SFMO sublattices.

S, %	ASD, %	Fe_{Fe}	Fe_{Mo}	Mo_{Mo}	Mo_{Fe}
100	0	1	0	1	0
90	5	0.95	0.05	0.95	0.05
80	10	0.9	0.1	0.9	0.1
70	15	0.85	0.15	0.85	0.15
60	20	0.8	0.2	0.8	0.2
50	25	0.75	0.25	0.75	0.25
40	30	0.7	0.3	0.7	0.3
30	35	0.65	0.35	0.65	0.35
20	40	0.6	0.4	0.6	0.4
10	45	0.55	0.45	0.55	0.45
0	50	0.5	0.5	0.5	0.5

Table 3. Ion occupation in the $Sr_2Fe_{0.95}Mo_{1.05}O_{6-\delta}$ sublattices.

S, %	ASD, %	Fe_{Fe}	Fe_{Mo}	Mo_{Mo}	Mo_{Fe}
100	0	0.95	0	1	0.05
90	5	0.9025	0.0475	0.9525	0.0975
80	10	0.855	0.095	0.905	0.145
70	15	0.8075	0.1425	0.8575	0.1925
60	20	0.76	0.19	0.81w	0.24
50	25	0.7125	0.2375	0.7625	0.2875
40	30	0.665	0.285	0.715	0.335
30	35	0.6175	0.3325	0.6675	0.3825
20	40	0.57	0.38	0.62	0.43
10	45	0.5225	0.4275	0.5725	0.4775
0	50	0.475	0.475	0.525	0.525

Table 4. Ion occupation in the $Sr_2Fe_{1.05}Mo_{0.95}O_{6-\delta}$ sublattices.

S, %	ASD, %	Fe_{Fe}	Fe_{Mo}	Mo_{Mo}	Mo_{Fe}
100	0	1	0.05	0.95	0
90	5	0.9525	0.0975	0.9025	0.0475
80	10	0.905	0.145	0.855	0.095
70	15	0.8575	0.1925	0.8075	0.1425
60	20	0.81	0.24	0.76	0.19
50	25	0.7625	0.2875	0.7125	0.2375
40	30	0.715	0.335	0.665	0.285
30	35	0.6675	0.3825	0.6175	0.3325
20	40	0.62	0.43	0.57	0.38
10	45	0.5725	0.4775	0.5225	0.4275
0	50	0.525	0.525	0.475	0.475

is treated using the Scherrer formula for full width at half maximum (FWHM) of the diffraction peak:

$$\mathrm{FWHM} = \frac{K\lambda}{d\cos\theta}, \quad (10)$$

where d is the average grain size, k a dimensionless coefficient of approximately 0.5 (for spherical particles), λ is the X-ray wavelength and θ is the diffraction angle. The calculated broadening of (112) and (200) peaks for 100 nm diameter spherical particles is 0.083°. This broadening further increases the total peak intensity (112) + (200) to 147.9% of the (112) peak intensity. The small lattice mismatch between SFMO and substrate only slightly changes the SFMO superstructure peak intensities. This was proved by additionally considering the lattice parameter combinations a = 0.557 nm with c = 0.804 nm, a = 0.562 nm with c = 0.792 nm and a = 0.795 nm with c = 0.560 nm simulating $SrTiO_3$, MgO and $LaAlO_3$ substrates, respectively [34]. The resulting curves slightly differ from the initial ones calculated for the lattice parameters a = 0.557 nm and c = 0.790 nm. The change in the lattice parameter due to oxygen vacancies [15, 35, 36] does not exceed the ones caused by SFMO/substrate lattice mismatch already considered above. Therefore, we have not examined it separately.

The calculated curves follow Eq. (2), but with the X axis data being compressed since the (404) peak intensity is lower than the (112) peak intensity. Therefore, we fitted our calculated curve with regard to Eq. (2) as follows:

$$\mathrm{ASD} = A - B\sqrt{\frac{I(101)}{[I(112)+I(200)]}}. \quad (11)$$

The parameter A is defined by the boundary condition: in disordered SFMO , i.e., for $I(101)/[I(112)+I(200)] \to 0$, A takes the value of 0.5. The parameter B equals to 2.318. The curve calculated using Eq. (11) is shown in Fig. 2.

Since the decrease in the (101) peak intensity is a measure of the concentration of Fe_{Mo} and Mo_{Fe} antisite pairs, the equilibrium condition

$$\mathrm{Fe_{Fe}} + \mathrm{Mo_{Mo}} \rightleftarrows \mathrm{Fe_{Mo}} + \mathrm{Mo_{Fe}}, \quad (12)$$

with the constant

$$k = [\mathrm{Fe_{Mo}}][\mathrm{Mo_{Fe}}] = [\mathrm{Fe_{Mo}}]^2, \quad (13)$$

yields a concentration of Fe_{Mo} and Mo_{Fe} antisite pairs in the form $k^{1/2}$ and hence, the decrease in the (101) peak intensity is the square root of the antisite pair concentration. Equation (11) allows express ASD evaluation from the (101) peak intensity and the sum of the (112) + (200) peak intensities.

For nonstoichiometric $Sr_2Fe_{1+x}Mo_{1-x}O_{6-\delta}$, the ASD is calculated by [24]:

$$\mathrm{ASD} = \frac{S_{\max} - S}{2}, \quad (14)$$

where S is the order parameter determined by Eq. (3) and S_{max} the maximum degree of superstructure order which, e.g. for SFMO with excess Mo, is determined by the formula:

$$S_{\max} = \mathrm{Fe_{Fe}} - \mathrm{Fe_{Mo}} = 2 - (\mathrm{Mo_{Mo}} + \mathrm{Mo_{Fe}}) < 1. \quad (15)$$

The intensities of the (112) and (200) peaks depend on instrumental error, grain size and degree of crystallinity. They are also affected by incorrect specimen preparation (specimen crushing, specimen holder preparation etc.). Nevertheless, the method of the degree of superstructure ordering from the ratio of the $I(101)/[I(112) + I(200)]$ peak intensities can be considered as a fairly simple evaluation method for SFMO compositions with the Fe/Mo ratio close to 1 since a peak intensity ratio is compared and the impact of the abovementioned factors was taken into account to a large extent.

4. Conclusion

In this work, an express method of ASD evaluation from the $I(101)/[I(112) + I(200)]$ peak intensity ratio by means of Eq. (11) was proposed. The method allows saving exposure time of the X-ray experiment and provides reliable results for near-stoichiometric SFMO specimens with Fe ≈ Mo.

Acknowledgements

The work was financially supported by the European Union within the Horizon 2020, H2020-MSCA-RISE-2017 Program (Grant No. 778308 SPINMULTIFILM).

References

1. Serrate D., De Teresa J.M., Ibarra M.R. Double perovskites with ferromagnetism above room temperature. *J. Phys.: Condens. Matter*, 2006; 19(2): 023201 (86pp). https://doi.org/10.1088/0953-8984/19/2/023201

2. Kobayashi K.-I., Kimura T., Sawada H., Terakura K., Tokura Y. Room-temperature magnetoresistance in an oxide material with an ordered double-perovskite structure. *Nature*, 1998; 395: 677–680. https://doi.org/10.1038/27167

3. Tomioka Y., Okuda T., Okimoto Y., Kumai R., Kobayashi K.-I., Tokura Y. Magnetic and electronic properties of a single crystal of ordered double perovskite Sr_2FeMoO_6. *Phys. Rev. B*, 2000; 61(1): 422–427. https://doi.org/10.1103/PhysRevB.61.422

4. Retuerto M., Alonso J.A., Martínez-Lope M.J., Martínez J.L., García-Hernández M. Record saturation magnetization, Curie temperature, and magnetoresistance in double perovskite synthesized by wet-chemistry techniques. *Appl. Phys. Lett.*, 2004; 85(2): 266–268. https://doi.org/10.1063/1.1772857

5. Suchaneck G., Kalanda N., Artsiukh E., Gerlach G. Challenges in Sr_2FeMoO_6 thin film deposition. *Phys. Status Solidi (b)*, 2019; 257(3): 1900312. https://doi.org/10.1002/pssb.201900312
6. Balcells Ll., Navarro J., Bibes M., Roig A., Martínez B., Fontcuberta J. Cationic ordering control of magnetization in Sr_2FeMoO_6 double perovskite. *Appl. Phys. Lett.*, 2001; 78: 781–783. https://doi.org/10.1063/1.1346624
7. Harnagea L., Berthet P. The effect of strontium non-stoichiometry on the physical properties of double perovskite Sr_2FeMoO_6. *J. Solid State Chem.*, 2015; 222: 115–122. https://doi.org/10.1016/j.jssc.2014.11.017
8. Fix T. *Couches minces de Sr_2FeMoO_6 élaborées par ablation laser pour des jonctions tunnel magnétiques*. Diss. Dr. Sci. (Phys.-Math.), Strasbourg, 2006.
9. Park B.J., Han H., Kim J., Kim Y.J., Kim C.S., Lee B.W. Correlation between anti-site disorder and magnetic properties in ordered perovskite Sr_2FeMoO_6. *J. Magnetism and Magnetic Materials*, 2004; 272(3): 1851–1852. https://doi.org/10.1016/j.jmmm.2003.12.429
10. Moritomo Y., Shimamoto N., Xu S., Machida A., Nishibori E., Takata M., Sakata M., Nakamura A. Effects of B-site disorder in Sr_2FeMoO_6 with double perovskite structure. *Jpn. J. Appl. Phys.*, 2001; 40(7A): L672–L674. https://doi.org/10.1143/JJAP.40.L672
11. Mishra R., Restrepo O.D., Woodward P.M., Windl W. First-principles study of defective and nonstoichiometric Sr_2FeMoO_6. *Chemistry of Materials*, 2010; 22(22): 6092–6102. https://doi.org/10.1021/cm101587e
12. Kalanda M., Suchaneck G., Saad A., Demyanov S., Gerlach G. Influence of oxygen stoichiometry and cation ordering on magnetoresistive properties of $Sr_2FeMoO_{6\pm\delta}$. *Materials Science Forum*, 2010; 636–637: 338–343. https://doi.org/10.4028/www.scientific.net/MSF.636-637.338
13. Momma K., Izumi F. VESTA 3 for three-dimensional visualization of crystal, volumetric and morphology data. *J. Appl. Cryst.*, 2011; 44: 1272–1276. https://doi.org/10.1107/S0021889811038970
14. Saloaro M., Deniz H., Huhtinen H., Palonen H., Majumdar S., Paturi P. The predominance of substrate induced defects in magnetic properties of Sr_2FeMoO_6 thin films. *J. Phys.: Condens. Matter*, 2015; 27: 386001 (11pp). https://doi.org/10.1088/0953-8984/27/38/386001
15. Kircheisen R., Töpfer J. Nonstoichiometry. Point defects and magnetic properties in $Sr_2FeMoO_{6-\delta}$ double perovskites. *J. Solid State Chem.*, 2015; 185: 76–81. https://doi.org/10.1016/j.jssc.2011.10.043
16. Wang J.-F., Li Z., Xu X.-J., Gu Z.-B., Yuan G.-L., Zhang S.-T. The competitive and combining effects of grain boundary and Fe/Mo antisite defects on the low-field magnetoresistance in Sr_2FeMoO_6. *J. American Ceramic Society*, 2014; 97: 1137–1142. https://doi.org/10.1111/jace.12749
17. Kuepper K., Balasz I., Hesse H., Winiarski A., Prince K.C., Matteucci M., Wett D., Szargan R., Burzo E., Neumann M. Electronic and magnetic properties of highly ordered Sr_2FeMoO_6. *Phys. Status Solidi (a)*, 2004; 201(15): 3252–3256. https://doi.org/10.1002/pssa.200405432
18. Sui Y., Wang X.J., Qian Z.N., Cheng J.G., Liu Z.G., Miao J.P., Li Y., Su W.H., Ong C.K. Enhancement of low-field magnetoresistance in polycrystalline Sr_2FeMoO_6 with doping. *Appl. Phys. Lett.*, 2004; 85(2): 269–271. https://doi.org/10.1063/1.1769581
19. Sarma D.D., Ray S., Tanaka K., Kobayashi A., Fujimori A., Sanyal P., Krishnamurthy H.R., Dasgupta C. Intergranular magnetoresistance in Sr_2FeMoO_6 from a magnetic tunnel barrier mechanism across grain boundaries. *Phys. Rev. Lett.*, 2007; 98: 157205 (4pp). https://doi.org/10.1103/PhysRevLett.98.157205
20. Hayes J. R., Grosvenor A. P. An investigation of the Fe and Mo oxidation states in $Sr_2Fe_{2-x}Mo_xO_6$ ($0.25 \le x \le 1.0$) double perovskites by *X*-ray absorption spectroscopy. *J. Alloys and Compounds*, 2012; 537: 323–331. https://doi.org/10.1016/j.jallcom.2012.05.056
21. Spiess L., Teichert G., Schwarzer R., Behnken H., Genzel C. *Moderne Röntgenbeugung: Röntgendiffraktometrie für Materialwissenschaftler, Physiker und Chemiker.* Berlin; Heidelberg; Wiesbaden: Springer Spektrum, 2019. 624 p. https://doi.org/10.1007/978-3-8348-8232-5
22. Izumi F., Momma K. Three-dimensional visualization in powder diffraction. *Solid State Phenomena*, 2007; 130: 15–20. https://doi.org/10.4028/www.scientific.net/SSP.130.15
23. Adeagbo W.A., Hoffmann M., Ernst A., Hergert W., Saloaro M., Paturi P., Kokko K. Tuning the probability of defect formation via substrate strains in Sr_2FeMoO_6 films. *Phys. Rev. Mater.*, 2018; 2(8): 083604 (9pp). https://doi.org/10.1103/PhysRevMaterials.2.083604
24. Liu G.Y., Rao G.H., Feng X.M., Yang H.F., Ouyang Z.W., Liu W.F., Liang J.K. Atomic ordering and magnetic properties of non-stoichiometric double-perovskite $Sr_2Fe_xMo_{2-x}O_6$. *J. Phys.: Condens. Matter*, 2003; 15(12): 2053–2060. https://doi.org/10.1088/0953-8984/15/12/322
25. Sánchez D., Alonso J.A., García-Hernández M., Martínez-Lope M.J., Martínez J.L., Mellergård A. Origin of neutron magnetic scattering in antisite-disordered Sr_2FeMoO_6 double perovskites. *Phys. Rev. B*, 2002; 65(10): 104426 (8pp). https://doi.org/10.1103/PhysRevB.65.104426
26. Navarro J., Frontera C., Rubi D., Mestres N., Fontcuberta J. Aging of Sr_2FeMoO_6 and related oxides. *Materials Research Bulletin*, 2003; 38(9–10): 1477–1486. https://doi.org/10.1016/S0025-5408(03)00171-5
27. Huang Y.H., Karppinen M., Yamauchi H., Goodenough J.B. Systematic studies on effects of cationic ordering on structural and magnetic properties in Sr_2FeMoO_6. *Phys. Rev. B*, 2006; 73(10): 104408 (5pp). https://doi.org/10.1103/PhysRevB.73.104408
28. Hu Y.C., Ge J.J., Ji Q., Lv B., Wu X.S., Cheng G.F. Synthesis and crystal structure of double-perovskite compound Sr_2FeMoO_6. *Powder Diffraction*, 2010; 25: S17–S21. https://doi.org/10.1154/1.3478711
29. Zhang Q., Xu Z.F., Wang L.F., Gao S.H., Yuan S.J. Structural and electromagnetic properties driven by oxygen vacancy in $Sr_2FeMoO_{6-\delta}$ double perovskite. *J. Alloys and Compounds*, 2015; 649: 1151–1155. https://doi.org/10.1016/j.jallcom.2015.07.211
30. Lü M., Li J., Hao X., Yang Z., Zhou D., Meng J. Hole doping double perovskites $Sr_2FeMo_{1-x}O_6$ (x = 0, 0.03, 0.04, 0.06) and their Mössbauer, crystal structure and magnetic properties. *J. Phys.: Condens. Matter*, 2008; 20(17): 175213 (9pp). https://doi.org/10.1088/0953-8984/20/17/175213
31. Kumar N., Gaur A., Kotnala R.K. Stable Fe deficient $Sr_2Fe_{1-\delta}MoO_6$ ($0 < \delta < 0.10$) compound. *J. Alloys and Compounds*, 2014; 601: 245–250. https://doi.org/10.1016/j.jallcom.2014.02.173
32. Wang J.-F., Zhang J., Hu B., Gu Z.-B., Zhang S.-T. Tunable low-field magnetoresistance in Sr_2FeMoO_6 ceramics using organic glycerin to modify grain boundaries and Fe/Mo ordering. *J. Phys. D: Appl. Phys.*, 2014; 47(44): 445003 (5pp). https://doi.org/10.1088/0022-3727/47/44/445003
33. Black D.R., Windover D., Henins A., Gil D., Filliben J., Cline J.P. Certification of NIST standard reference material 640d. *Power Diffraction*, 2010; 25(2): 187–190. https://doi.org/10.1154/1.3409482

34. Jalili H., Heinig N.F., Leung K.T. Growth evolution of laser-ablated Sr_2FeMoO_6 nanostructured films: Effects of substrate-induced strain on the surface morphology and film quality. *J. Chem. Phys.*, 2010; 132: 204701 (7pp). https://doi.org/10.1063/1.3407453

35. Agata S., Moritomo Y., Machida A., Kato K., Nakamura A. Oxidization control of transport properties of $Sr_2FeMoO_{6+\delta}$ film. *Jpn. J. Appl. Phys.*, 2002; 41: L688–L 690. https://doi.org/10.1143/JJAP.41.L688

36. Kalanda N., Turchenko V., Karpinsky D., Demyanov S., Yarmolich M., Balasoiu M., Lupu N., Tyutyunnikov S., Sobolev N. A. The role of the Fe/Mo cations ordering degree and oxygen non-stoichiometry on the formation of the crystalline and magnetic structure of $Sr_2FeMoO_{6-\delta}$. *Phys. Status Solidi B*, 2018; 256: 1800278 (7pp). https://doi.org/10.1002/pssb.201800278